Toward a Reliable Correction of NOAA AVHRR Orbital Drift

Yves Julien* and José A. Sobrino

Global Change Unit, Image Processing Laboratory, University of Valencia, Valencia, Spain

The NOAA (National Oceanic and Atmospheric Administration) AVHRR (Advanced Very High-Resolution Radiometer) orbital drift prevents the use of its derived land surface temperature (LST) data for global studies of temperature trends, especially for the 80s and 90s over land. In a previous study, we showed how orbital drift correction methods could be validated by simulating a reference and drifted time series from alternative MSG (Meteosat Second Generation) SEVIRI (Spinning Enhanced Visible and InfraRed Imager) data, thanks to their high (15 min) temporal resolution. In this study, we show how these alternative data allow identifying orbital drift effects on different land covers, and how these effects could be mitigated with novel approaches. We also identify two key statistical parameters to assess orbital drift correction performance: the bias between corrected and drifted time series and the trend of their difference. We present two methods and compare their results with an alternative orbital drift correction, validated against *in situ* data by their authors. Considering an ideal case where the whole influence of the orbital drift is known, our novel approach allows for an almost complete removal of the orbital drift effect (zero bias and 0.05 K/yr difference trend). However, in real cases, when we have only access to the drifted time series, our approach's performance decreases slightly, mainly through a larger spread of the retrieved statistics. As for the alternative correction method, its performance is poorer, even if it actually succeeds in removing part of the observed orbital drift. These results, as well as the new insights we provide on the orbital drift effect on LST, pave the way toward a reliable correction of NOAA AVHRR orbital drift. We therefore recommend the use of simulated LST time series such as the ones used in this study for the validation of orbital drift correction methods.

Keywords: LST, SEVIRI, MSG, time series, temperature

1 INTRODUCTION

Despite providing the longest daily record of remotely sensed thermal data (more than 40 years), the NOAA (National Oceanic and Atmospheric Administration) AVHRR (Advanced Very High-Resolution Radiometer) dataset has been underutilized as regards its thermal component, due to the orbital drift the NOAA platforms suffer (Price, 1990). For the afternoon satellites (NOAA-7, 9, 11, 14, 16, 18, and 19), this orbital drift consists in a progressively later overpass (see **Figure 1**), and their nominal orbit being set to coincide roughly with maximum surface temperature; this results in decreasing temperatures throughout the lifetime of each satellite. This orbital drift effect hides the actual changes in surface temperature, while these changes in surface temperature would be extremely useful for climate studies. Indeed, the NOAA AVHRR dataset starts in July 1981 and covers the decades for which climate warming has soared and provides information over the whole
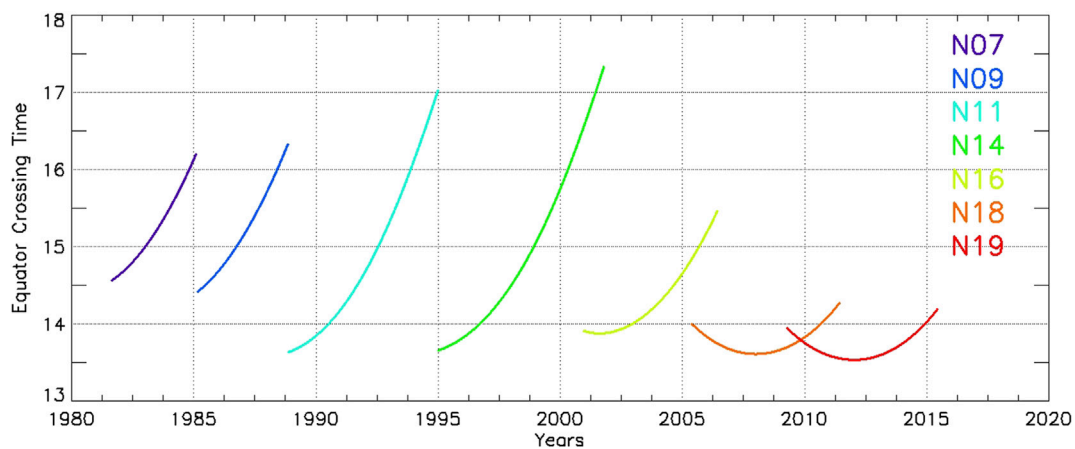
FIGURE 1 | Equatorial crossing times for the NOAA afternoon platforms simulated in this work.

world, filling the lack of data over wide areas of our planet (mostly in the Southern Hemisphere), especially in the 80s and 90s.

Of course, the literature offers several methods to overcome this orbital drift effect. As stated in a previous work (Julien and Sobrino, 2021), these methods can be classified into three groups: sun–target–sensor geometry modeling, land surface temperature (LST) diurnal cycle reconstruction, and statistical methods. The first group uses vegetation structure models to estimate the proportion of shaded and lit areas to estimate each pixel LST for each NOAA overpass (Pinheiro et al., 2004). This approach has been used to build a daily record of NOAA-14 AVHRR LST over Africa (Pinheiro et al., 2006). The second group relies on the reconstruction of the LST diurnal cycle, which allows, once identified, retrieval of the LST that would have been measured at a given hour (Susskind et al., 1997; Jin and Treadon, 2003; Liu et al., 2019). The reconstruction of the LST diurnal cycle is the key aspect of this approach and can be carried out from modeling (Jin and Treadon, 2003), interpolation from several measurements through the same day (Susskind et al., 1997), or a local neighborhood (Liu et al., 2019), under the assumption of local similarity of surface characteristics. The third group relies on time series analysis and uses the drifted LST time series to isolate the drift from a proxy signal, usually the solar zenith angle (SZA), to represent the image acquisition time (Gutman, 1999; Pinzon et al., 2005; Sobrino et al., 2008; Julien and Sobrino, 2012).

However, these orbital drift correction methods have been seldom validated. At best, comparison of time series statistics before and after the correction was used to show the improvement in time series consistency. Recently, an orbital drift correction method was proposed and validated by comparison with independent ground data (Liu et al., 2019). However, validation is a difficult task due to the large footprint of the NOAA AVHRR pixel in available datasets (around 5–8 km) and the lack of representativity of point measurements over such a wide area, not to mention the lack of consistent *in situ* measurements over 40 years of time. As a result, Liu et al.'s (2019) validation shows an error up to 3 K. Such values are expected in the case of LST validation from the AVHRR

instrument but may not inform on the actual removal of orbital drift effects. Actually, LST, as an essential climate variable (ECV), is expected to be retrieved with an uncertainty below 1 K and a long-term stability below 0.1 K per decade (or 0.01 K per year).

To bridge this gap, we showed in a previous work (Julien and Sobrino, 2021) how orbital drift correction methods could be validated by using an alternative data source, namely, the MSG (Meteosat Second Generation) SEVIRI (Spinning Enhanced Visible and InfraRed Imager) LST dataset. Due to its high temporal resolution (15 min) and its similar spatial resolution (3 km at nadir), SEVIRI LST can be used to simulate both a reference and a drifted dataset, in the latter case, by applying Ignatov et al. (2004) equations for equatorial crossing time determination of different NOAA platforms. To see the effect of orbital drift on various land covers, we constructed such time series for the BELMANIP sites (Baret et al., 2006) located in the SEVIRI observational disk. Then it is only a matter of correcting the drifted time series with the chosen orbital drift correction method and comparing it to the reference time series (see **Section 2**).

Building on this previous work, we propose here to exploit these drifted and reference time series for the analysis of the orbital drift effect on LST, to find a general expression of this drift, and to design an operational method for its correction (**Section 3**). This operational correction is then validated and compared with Liu et al.'s (2019) approach (**Section 4**). Finally, advantages and flaws of this operational correction are discussed (**Section 5**).

2 DATA

Although the aim of this study was to correct the NOAA AVHRR orbital drift effect on LST, we did not use any AVHRR data in this study. Since ground LST data for early NOAA satellites (80s and 90s) are at best seldom, there is no *in situ* LST information to validate AVHRR LSTs, and proxy data, such as air temperature, are available after modeling and at a coarser spatial resolution

(such as REANALYSIS or WATCH data, see, respectively, Herschbach et al. (2020) and Weedon et al. (2011)). Therefore, to validate our approach, we settled for the use of MSG-SEVIRI LST data.

The SEVIRI sensor, on geostationary MSG satellite series since 2007, provides information for half the planet, centered at the (0°, 0°) latitude and longitude points, every 15 min. Its spatial resolution is 3 × 3 km at nadir, spreading roughly 4 × 5 km over Southern Europe, for example. The SEVIRI instrument provides data on 12 spectral channels: four in the visible and near-infrared wavelengths (0.4–1.6 μm) and eight in the infrared wavelengths (3.9–13.4 μm). These bands are termed high-resolution visible (HRV; with higher spatial resolution: 1 × 1 km at nadir), VIS06, VIS08, IR016, IR039, WV062, WV073, IR087, IR097, IR108, IR120, and IR134. Bands WV6.2 and WV7.3 are located in a water vapor (WV) absorption region, whereas band IR9.7 is located in the ozone absorption region and band IR134 in a CO_2 absorption region. The other bands are located in regions with high atmospheric transmissivity (atmospheric windows); in particular, bands IR108 and IR120 are located in the split-window region and are used for surface and cloud observation. These two thermal bands are similar to the ones of the AVHRR instrument. Moreover, the MSG-SEVIRI spatial footprint is similar to the data available from the AVHRR datasets (LTDR-V5: Long-Term Data Record version 5; Pedelty et al., 2007) and can provide LST values for half our planet every 15 min, therefore allowing an adequate simulation of AVHRR drifted and reference LST time series.

Since 2007, the Global Change Unit of the University of Valencia operates a receiving station for MSG-SEVIRI data and processes routinely the received data for the estimation of NDVI (Normalized Difference Vegetation Index), SST (sea surface temperature), and LST parameters. The whole processing scheme of the data received by our MSG-SEVIRI station is described in Julien et al. (2015), while the LST and SST algorithms are presented in Sobrino et al. (2020c). In summary, this process consists in retrieving brightness temperatures for IR108 and IR120 bands, from which surface temperatures are estimated through the split-window approach, through a previous estimation of emissivities and total atmospheric water vapor (Julien et al., 2015; Sobrino et al., 2020c).

Here, as for our previous study (Julien and Sobrino, 2021), we used the LST data we retrieved at our premises for the years 2013–2019. Additionally, for comparison purposes with the Liu et al. (2019) method, we retrieved daily maximum NDVI for the same period. Finally, we downloaded MSG-SEVIRI cloud masks from the EUMETSAT archive for the years 2013–2019. These masks are built following the methodology developed by Derrien and Le Gléau (2005). The masks are provided for pixels with a viewing zenith angle below 80°, whose values 0, 1, 2, and 3 correspond, respectively, to clear over sea, clear over land, cloudy, and no data. In this work, we only used LST estimations corresponding to cloud mask values of 1. Cloud mask values before 2016 are unavailable for pixels with a viewing zenith angle above 73°.

For visualization purposes and to save computer memory as well as processing time, we selected all Benchmark Land Multisite

Analysis and Intercomparison of Products (BELMANIP; Baret et al., 2006) sites included in the MSG-SEVIRI disk, provided their viewing zenith angle was below 73° (177 in total). The locations of these pixels are provided in **Figure 2** along with the International Geosphere Biosphere Programme (IGBP) class associated to the corresponding BELMANIP site. Corresponding MSG-SEVIRI pixels may include a possible mix of land cover classes, although the labeled land cover class is expected to be predominant. The number of available sites within each class is presented in **Table 1**.

3 METHODS

The approach presented here is a statistical correction of the orbital drift effect. Since the orbital drift has a different effect on surface temperature depending on pixel latitude, land cover, and daily and yearly temperature amplitudes, we chose a statistical approach consisting in fitting the orbital drift effect against a generic equation with parameter values varying for each pixel characteristic.

Since the specifics of the building of reference and drifted LST time series are detailed in Julien and Sobrino (2021), we provide here only a summary of the approach. First, we need to choose a reference hour for the reference time series. We tested different hours (13:30, 14:00, and 14:30 solar time); although for operational purposes, the average of the equatorial crossing times over the first year of each platform was chosen ($AEXT_0$). These reference hours are estimated using Ignatov et al. (2004) equatorial crossing time equations, and are presented in **Table 2**, along with different platform characteristics (start of activity period (SAP) and end of activity period (EAP), as retrieved from the LTDR-V4 dataset, as well as the date of the first available data (FAD)).

Since no MSG-like data are available before 2007, we used the period 2013–2019 to simulate the daily overpass hour for all NOAA platforms for each BELMANIP site of **Figure 1**. The year 2019 was chosen as the end date of the SEVIRI LST time series, conserving the DOY of the end of activity period in order to respect eventual seasonal effects on the orbital drift. Finally, daily LST values were retrieved linearly from the closest two observations (LST_{DRIFT}). When any (or both) of these two neighboring measurements were labeled as cloudy, we also labeled the interpolated LST value as cloudy. We proceeded similarly for the reference LST time series (LST_{REF}). For comparison purposes, we retrieved these LST time series also for a 9 × 9 neighborhood of each BELMANIP location and daily NDVI maximum value for this same neighborhood. In that case, and according to the reference study (Liu et al., 2019), the reference overpass time was set to 14:30 (solar time).

To assess the effectiveness of orbital drift correction, the few studies available to date have used statistics such as bias, standard deviation (STDV), and root mean square error (RMSE). Here, we propose an alternative approach, by calculating, for each site and each NOAA platform, the difference between the corrected and the reference time series and then retrieving the lineal trend of
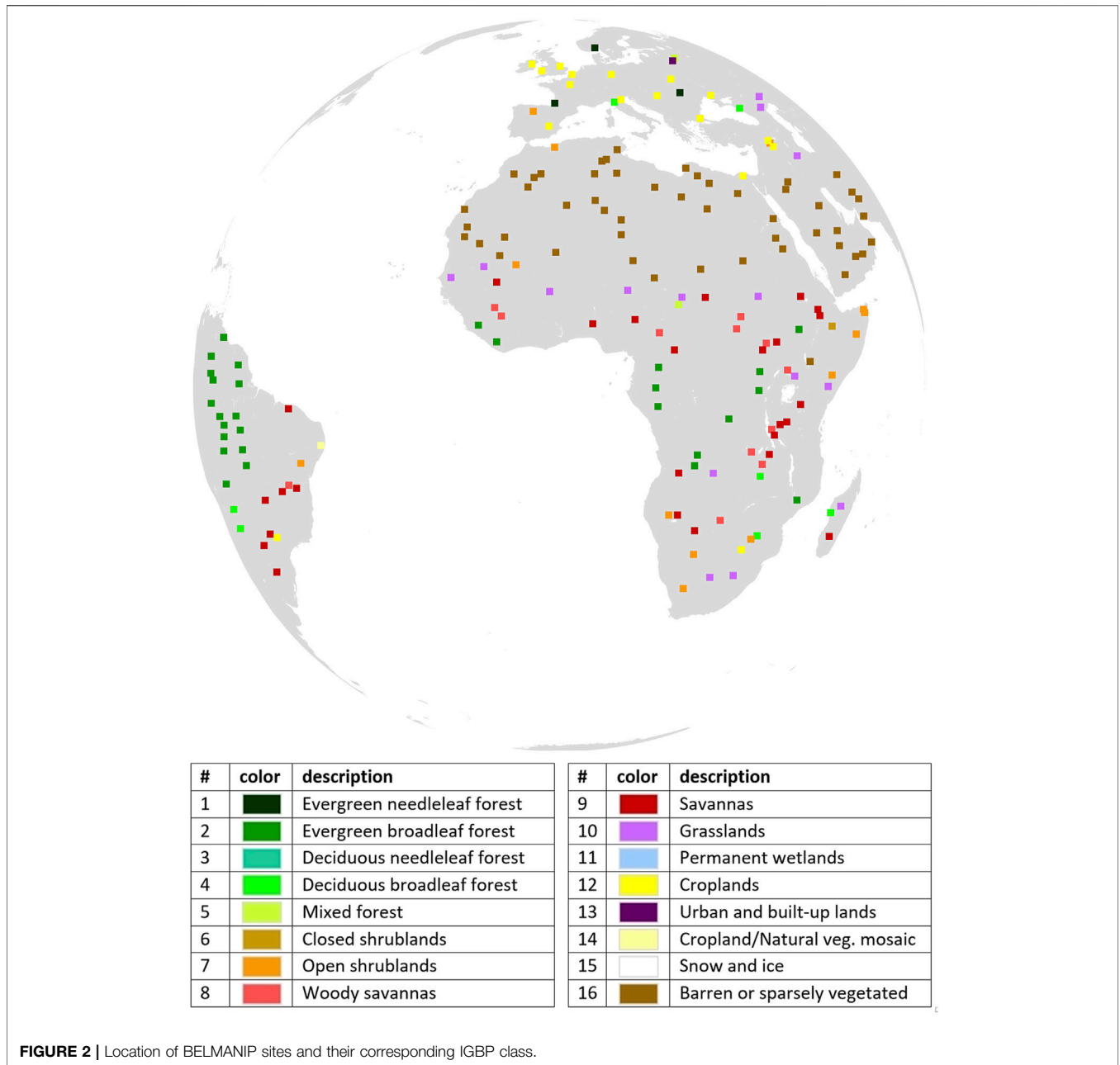
FIGURE 2 | Location of BELMANIP sites and their corresponding IGBP class.

#	color	description		#	color	description
1		Evergreen needleleaf forest		9		Savannas
2		Evergreen broadleaf forest		10		Grasslands
3		Deciduous needleleaf forest		11		Permanent wetlands
4		Deciduous broadleaf forest		12		Croplands
5		Mixed forest		13		Urban and built-up lands
6		Closed shrublands		14		Cropland/Natural veg. mosaic
7		Open shrublands		15		Snow and ice
8		Woody savannas		16		Barren or sparsely vegetated

TABLE 1 | Number of BELMANIP sites for each IGBP class. Classes with no corresponding sites were removed from the table for brevity (classes 3, 11, and 15).

Class	1	2	4	5	6	7	8	9	10	12	13	14	16
Sites	3	28	7	2	1	13	12	26	15	17	1	1	51
Selected	244	156	120	188	–	139	–	–	137	–	–	40	208

this difference (TREND). Additionally, we retrieve the correlation value between both time series (CORR).

With regard to the orbital drift influence on LST time series, we estimated, for each site and each satellite, the difference between the reference and drifted time series. **Figure 3** presents this difference for site 208 and the NOAA-11 platform. We can observe a clear increase in the difference with time, modulated by a seasonal signal, whose amplitude also increases with time. This temporal behavior is similar for all pixels, with varying seasonal signals and amplitudes (not shown for brevity).

TABLE 2 | Characteristics of NOAA platforms. $AEXT_0$: average of the equatorial crossing times over the first year of each platform; SAP: start of activity period; EAP: end of activity period; FAD: first available data.

Platform	NOAA-7	NOAA-9	NOAA-11	NOAA-14	NOAA-16	NOAA-18	NOAA-19
$AEXT_0$ (h)	14.6944	14.5639	13.7073	13.7260	13.8842	13.8687	13.8096
SAP	24/08/1981	25/02/1985	08/11/1988	01/01/1995	18/12/2000	17/05/2005	14/04/2009
EAP	01/02/1985	07/11/1988	31/12/1994	15/10/2001	31/12/2005	31/12/2009	02/10/2015
FAD	23/06/1981	12/12/1984	25/02/1989	30/12/1994	21/09/2000	20/05/2005	06/02/2009
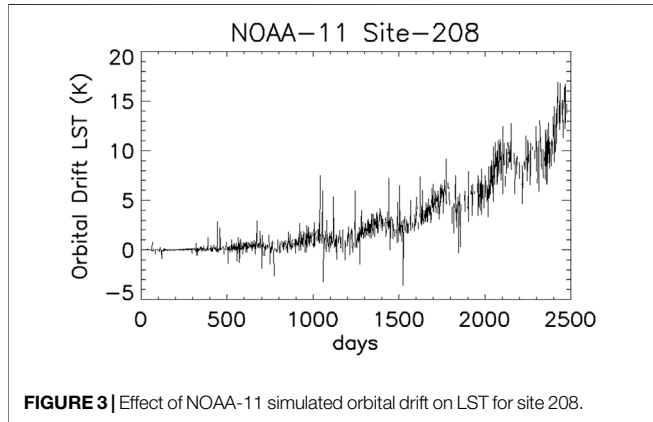
FIGURE 3 | Effect of NOAA-11 simulated orbital drift on LST for site 208.

Based on this observation, we propose the following formulation for the orbital drift effect (Δ_{LST}):

$$\Delta_{LST}(t) = s(t) * (h_{REF} - h_{DRIFT}) + a + b \cdot d(t), \quad (1)$$

where t is time (in days), $s(t)$ is a seasonal signal to be defined, h_{REF} is the reference equator crossing time (in hours), h_{DRIFT} is the drifted equator crossing time (in hours), a and b are fit coefficients, and $d(t)$ is the drift signal, as estimated from Ignatov et al. (2004), as follows:

$$d(t) = \alpha_1 \sin\left(\omega_1(t - t_0) + \varphi_1\right) + \alpha_2 \sin\left(\omega_2(t - t_0) + \varphi_2\right), \quad (2)$$

where α_1, ω_1, φ_1, α_2, ω_2, and φ_2 are fit coefficients retrieved by Ignatov et al. (2004) and available for download at https://www.star.nesdis.noaa.gov/socd/sst/3s/(tab labeled as EXT). As for t_0, its value is set, for each platform, to the difference between the first available data (FAD) and the start of activity period (SAP).

In the aforementioned equations, the unknowns are $s(t)$, a, and b. To retrieve them, we proceed iteratively, by first estimating a and b by fitting $\Delta_{LST}(t)$ against $d(t)$ using a Levenberg–Marquardt approach and then by the estimation of $s(t)$ as the average year of $\frac{\Delta_{LST}(t) - (a + b \cdot d(t))}{(h_{REF} - h_{DRIFT})}$, smoothed over 60 days to remove discontinuities. This step can be carried out satellite by satellite or considering all satellites at the same time. Since it leads to better performance, we present here only the results when this step is carried out considering all satellites together. Then in a second iteration, $\Delta_{LST}(t) - s(t) * (h_{REF} - h_{DRIFT})$ is fitted against $d(t)$, followed by the second step mentioned earlier. This iterative process allows us to refine the estimates of $s(t)$, a, and b, until the maximum difference between two iterations is below 0.05 K.

This procedure corresponds to the ideal case, when both the reference and drifted time series are available; therefore, we have

$\Delta_{LST}(t) = LST_{REF}(t) - LST_{DRIFT}(t)$. However, for practical cases, only the drifted time series is available, and therefore $\Delta_{LST}(t)$ has to be guessed approximatively. Considering that for each platform, its first year of activity was the year with a lower orbital drift effect—this is especially verified for NOAA-7, 9, 11, and 14, and to a lesser extent for the last three platforms—we can use $\Delta_{LST}(t) = LST_{DRIFT}(t) - LST_{DRIFT}^{y0}(t)$, where $LST_{DRIFT}^{y0}(t)$ is the smoothed (over 60 days) drifted LST during the first year activity of the platform, replicated to cover the whole activity period. This is the equivalent of the anomaly of the drifted LST from its first year. However, in that case, the seasonal component of the drift is lost within the day-to-day variations in LST, and recovering it is a challenging task. So, a simple Levenberg–Marquardt fit is carried out to retrieve the value of coefficients a and b, while $s(t)$ is set fixed to zero.

Finally, for comparison purposes, we implemented the orbital drift correction approach described in Liu et al. (2019). This approach is based on the estimation of the daily temperature cycle at a given location by using a local neighborhood (3×3 or 9×9) to retrieve the five coefficients needed to describe this daily temperature cycle. These coefficients are then used to estimate the corrected LST at this pixel at the reference time. All the specifics of the approach are detailed in Liu et al. (2019) and were implemented thoroughly for our comparison.

4 RESULTS

4.1 Overall Statistics

First, to decide which statistics are best suited for orbital drift correction effectiveness, we present in **Table 3** different parameters retrieved by comparison of the drifted LST time series and the reference LST time series, averaged over all sites, for each satellite, over NOAA-7 to 11 platforms, and over all platforms. We observe a clear difference between the four first NOAA platforms (7–11) and the last three, which had orbits carefully chosen so that the drift was lower during the first years of the activity period (see **Figure 1**). For the last two platforms especially, bias and difference trend are close to zero, standard deviation and RMSE are of the order of 0.7 K, while correlation is high (0.99). However, for the platforms with the strongest orbital drift (NOAA-7 to 11), bias can reach −2 K and below, and STDV almost 3.6 K, resulting in an RMSE above 4 K. Difference trends are negative, as expected, and are close to −1.5 K per year, while correlations can drop below 0.90. However, these statistics are not independent, and besides the well-known relationship between bias, standard deviation, and RMSE, the

TABLE 3 | Statistical assessment of the orbital drift effect on LST for each NOAA platform, for NOAA-7 to 14 platforms, and overall: average value over all sites with its standard deviation in parentheses. STDV: standard deviation; RMSE: root mean square error; TREND: the lineal trend of the difference between drifted and reference time series; CORR: the correlation value between both time series.

Platform	BIAS (K)	STDV (K)	RMSE (K)	TREND (K/yr)	CORR
NOAA-7	−1.30 (0.76)	1.90 (0.54)	2.36 (0.76)	−1.44 (0.82)	0.94 (0.05)
NOAA-9	−1.53 (0.90)	2.14 (0.65)	2.69 (0.95)	−1.52 (0.86)	0.93 (0.06)
NOAA-11	−1.99 (1.27)	3.12 (1.08)	3.78 (1.47)	−1.36 (0.79)	0.88 (0.08)
NOAA-14	−2.36 (1.43)	3.59 (1.24)	4.39 (1.67)	−1.43 (0.79)	0.86 (0.10)
NOAA-16	−0.59 (0.41)	1.27 (0.38)	1.43 (0.46)	−0.49 (0.33)	0.97 (0.03)
NOAA-18	0.04 (0.09)	0.67 (0.31)	0.68 (0.31)	−0.03 (0.04)	0.99 (0.02)
NOAA-19	0.05 (0.10)	0.67 (0.32)	0.67 (0.32)	−0.02 (0.04)	0.99 (0.02)
N7-14	−1.80 (1.19)	2.69 (1.16)	3.31 (1.51)	−1.44 (0.82)	0.90 (0.08)
All	−1.10 (1.24)	1.91 (1.29)	2.29 (1.67)	−0.90 (0.90)	0.94 (0.08)

TABLE 4 | Statistical assessment of our orbital drift correction method in the ideal case for each NOAA platform, for NOAA-7 to 14 platforms, and overall: average value over all sites with its standard deviation in parentheses. TREND: the lineal trend of the difference between drifted and reference time series.

Platform	BIAS (K)	TREND (K/yr)
NOAA-7	−0.00 (0.07)	0.01 (0.10)
NOAA-9	−0.00 (0.08)	0.01 (0.12)
NOAA-11	−0.00 (0.08)	0.07 (0.11)
NOAA-14	0.01 (0.07)	0.12 (0.08)
NOAA-16	0.01 (0.06)	0.06 (0.06)
NOAA-18	0.00 (0.04)	−0.00 (0.02)
NOAA-19	−0.00 (0.04)	−0.00 (0.02)
N7-14	0.00 (0.08)	0.04 (0.09)
All	0.00 (0.07)	0.05 (0.06)

TABLE 6 | Statistical assessment of Liu et al. (2019) orbital drift correction method for each NOAA platform, for NOAA-7 to 14 platforms, and overall: average value over all sites with its standard deviation in parentheses. TREND: the lineal trend of the difference between drifted and reference time series.

Platform	BIAS (K)	TREND (K/yr)
NOAA-7	−0.04 (3.41)	−0.74 (1.42)
NOAA-9	0.13 (3.48)	−0.59 (1.64)
NOAA-11	1.04 (2.56)	−0.96 (1.76)
NOAA-14	0.78 (2.93)	−0.99 (1.71)
NOAA-16	1.80 (1.48)	−0.39 (1.19)
NOAA-18	2.55 (2.40)	−0.13 (0.24)
NOAA-19	2.70 (2.51)	−0.12 (0.27)
N7-14	0.48 (3.14)	−0.82 (1.64)
All	1.28 (2.93)	−0.56 (1.36)

TABLE 5 | Statistical assessment of our orbital drift correction method in the real case for each NOAA platform, for NOAA-7 to 14 platforms, and overall: average value over all sites with its standard deviation in parentheses. TREND: the lineal trend of the difference between drifted and reference time series.

Platform	BIAS (K)	TREND (K/yr)
NOAA-7	−0.19 (0.62)	0.12 (0.54)
NOAA-9	0.00 (0.69)	−0.08 (0.47)
NOAA-11	−0.24 (0.88)	0.02 (0.27)
NOAA-14	−0.09 (0.95)	0.01 (0.22)
NOAA-16	−0.22 (0.89)	−0.04 (0.30)
NOAA-18	−0.29 (0.81)	−0.02 (0.10)
NOAA-19	−0.29 (0.83)	−0.02 (0.08)
N7-14	−0.03 (0.81)	0.02 (0.40)
All	−0.13 (0.83)	−0.00 (0.33)

difference trend is integrated in the standard deviation, alongside the uncertainty in LST measurement. As a matter of fact, most standard deviation values are below or around 2 K, which is roughly the uncertainty in LST estimation (see, for example, Sobrino et al., 2020c). On the other hand, bias and difference estimates depart considerably from zero and display all the influence of the orbital drift. As for correlation, its value remains high in all cases, and the amplitude of its variation may be too small for our purposes. Thus, we will focus on bias and difference trend statistics hereafter.

Table 4 displays the bias and difference trend statistics for the ideal case, that is, when both drifted and reference time series are

available for the correction. We see that our correction, in this ideal case, performs adequately, with close to zero bias values and low difference trend values overall. However, these trend values are slightly higher for NOAA-11, 14, and 16 platforms (around 0.10 K/yr), even though the error has been decreased by a factor 10 (see **Table 4**).

Table 5 presents the bias and difference trend statistics for the real case, that is, when reference time series are not available for the time series correction. We see that our correction, in this real case, performs slightly worse, with higher mean bias values with higher variability. As for difference trend values, their average is similar to that of the ideal case, although with a higher heterogeneity (overall trend difference standard deviation around 0.33 K/yr). Again, these trend values are slightly higher, this time for NOAA-7 and 9 platforms (around 0.10 K/yr).

Table 6 presents the bias and difference trend statistics for the correction of Liu et al. (2019), as described in the Methods section. We see that this correction decreases the bias and difference trend values when compared with the drifted time series, with better success in these latter for NOAA-16, 18, and 19, although this method falls short from removing the orbital drift completely.

4.2 Selected Sites
For visualization purposes, we selected eight sites among the 177 BELMANIP sites located within MSG-SEVIRI disk. **Table 7**

TABLE 7 | Characteristics of the eight sites selected for visualization purposes.

Site	Class number	Class	Latitude	Longitude	% Clouds
40	14	Crop/vegetation mosaic	−8.403	−35.607	89.9
120	4	Broadleaf deciduous forest	−21.421	30.445	66.7
137	10	Grassland	−12.075	21.582	71.4
139	7	Open shrubland	−17.956	15.504	46.2
156	2	Broadleaf evergreen forest	7.774	35.293	95.7
188	5	Mixed forest	10.967	16.339	72.1
208	16	Desert	25.159	22.711	33.4
244	1	Needleleaf evergreen forest	43.860	−1.099	83.7

FIGURE 4 | Simulated time series for NOAA-11 platform for eight selected sites: reference (black) and drifted (red) time series along with the resulting bias and trend difference statistics.
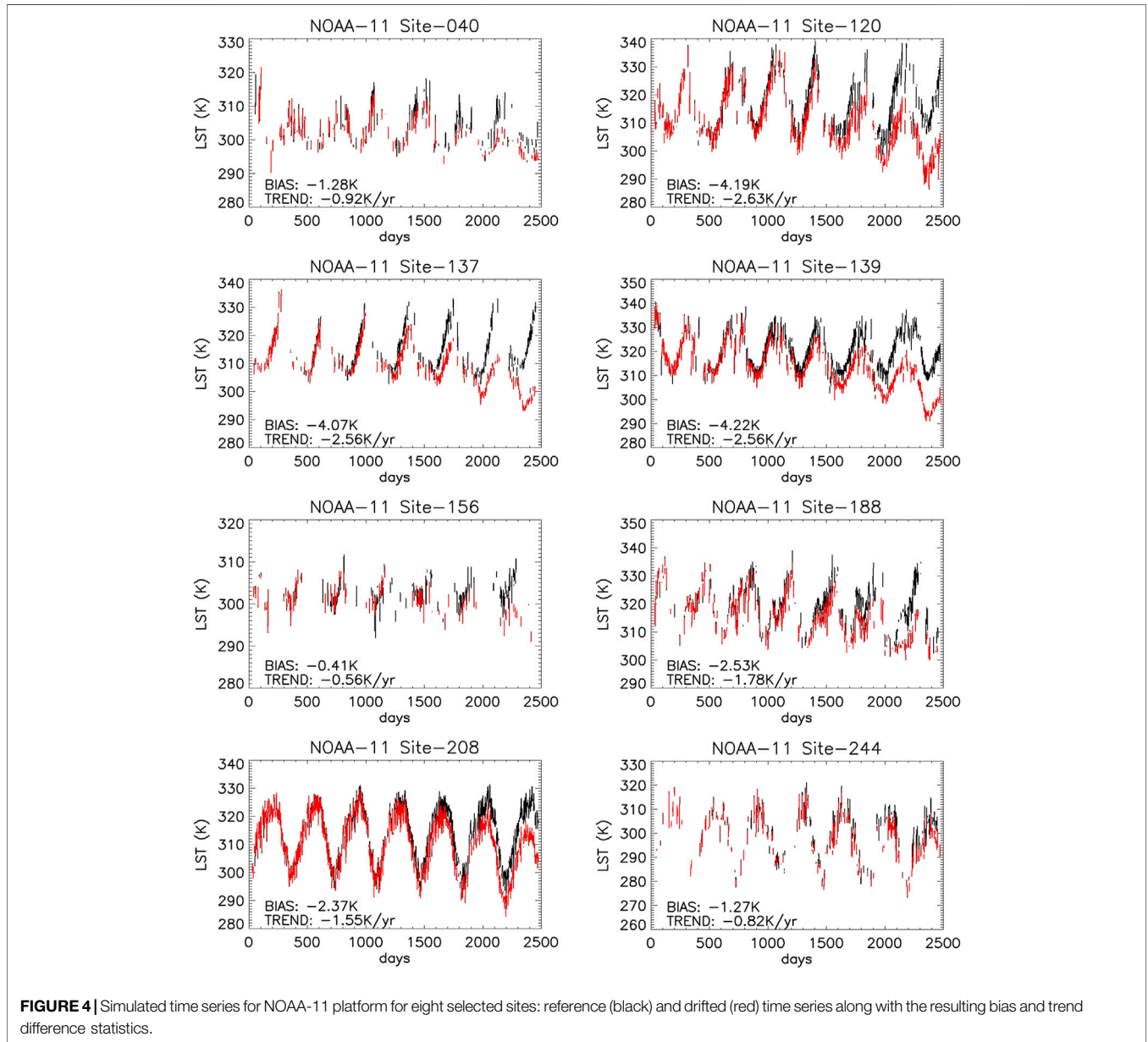
presents the characteristics of these eight sites, such as site number, corresponding IGBP class number and land cover, site latitude, and longitude, as well as the percentage of cloudy pixels over the NOAA-11 activity period. Note that for only two of these sites the percentage of cloudy observations is below 50% (sites 139 and 208).

FIGURE 5 | Corrected time series for NOAA-11 platform for eight selected sites: reference (black) and ideal case corrected (green) time series along with the resulting bias and trend difference statistics.
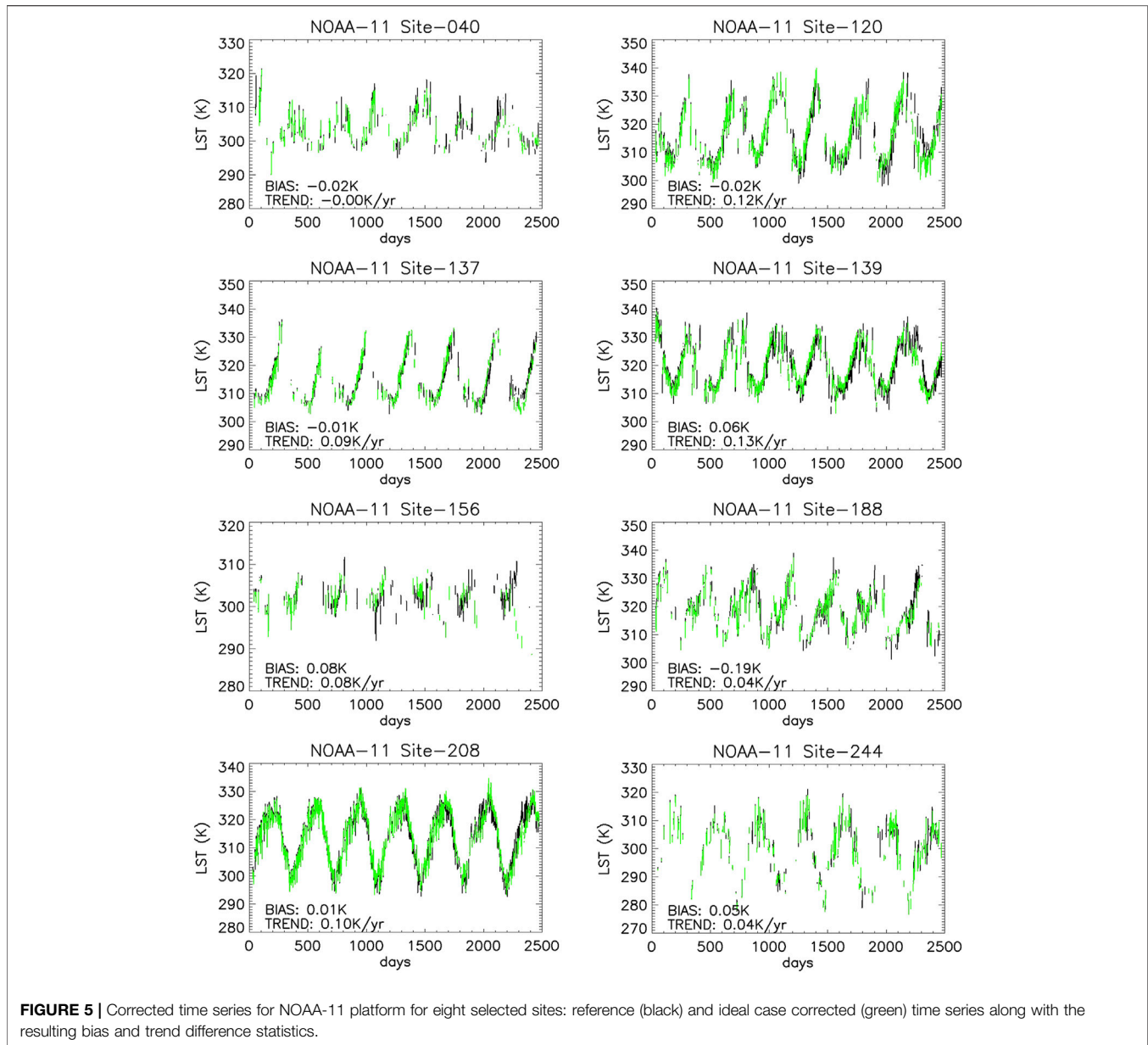
Figure 4 displays bias and trend difference statistics for the eight sites, as described in **Table 7**, for reference and drifted NOAA-11 simulated data. We see that for five of these sites (120, 137, 139, 188, and 208), the influence of the orbital drift can be detected visually, while the bias and trend difference statistics show substantial deviations from zero for all sites. We also see that the sites with higher absolute bias values (above 2 K) correspond to the following classes: broadleaf deciduous forest, grassland, open shrubland, mixed forest, and desert. These sites are also the ones evidencing the lowest trend difference values (below −1 K/yr). However, we observe that NOAA orbital drift influences retrieved statistical parameters for all selected sites.

Figure 5 presents the same statistical parameters after our orbital drift correction in the ideal case (reference time series available for correction). At first glance, we see that the reference and corrected

time series have a similar behavior. We observe a clear reduction in both bias and trend difference values, with bias values ranging from −0.19 to 0.08 K and trend difference values from 0 to 0.13 K/yr.

As for the real case (reference time series unavailable for correction), we also observe (**Figure 6**) a similar behavior for both reference and corrected time series, with small deviations for site 137. We see a clear increase of the bias statistics, with values ranging from −3.40 to 0.97 K. Regarding the trend statistics, it also increases, with values ranging from −0.29 to 0.59 K/yr. Note that for the desert site, with lower cloud contamination, the remaining trend is 0.03 K/yr.

Finally, the same statistical parameters were retrieved for the same sites for Liu et al. (2019) correction (**Figure 7**). Visually, a remaining orbital drift is evident for all sites, except maybe site 40. For all sites, the trend difference absolute value remains high, ranging between −2.70 and 1.05 K/yr.

FIGURE 6 | Corrected time series for NOAA-11 platform for eight selected sites: reference (black) and real case corrected (blue) time series along with the resulting bias and trend difference statistics.
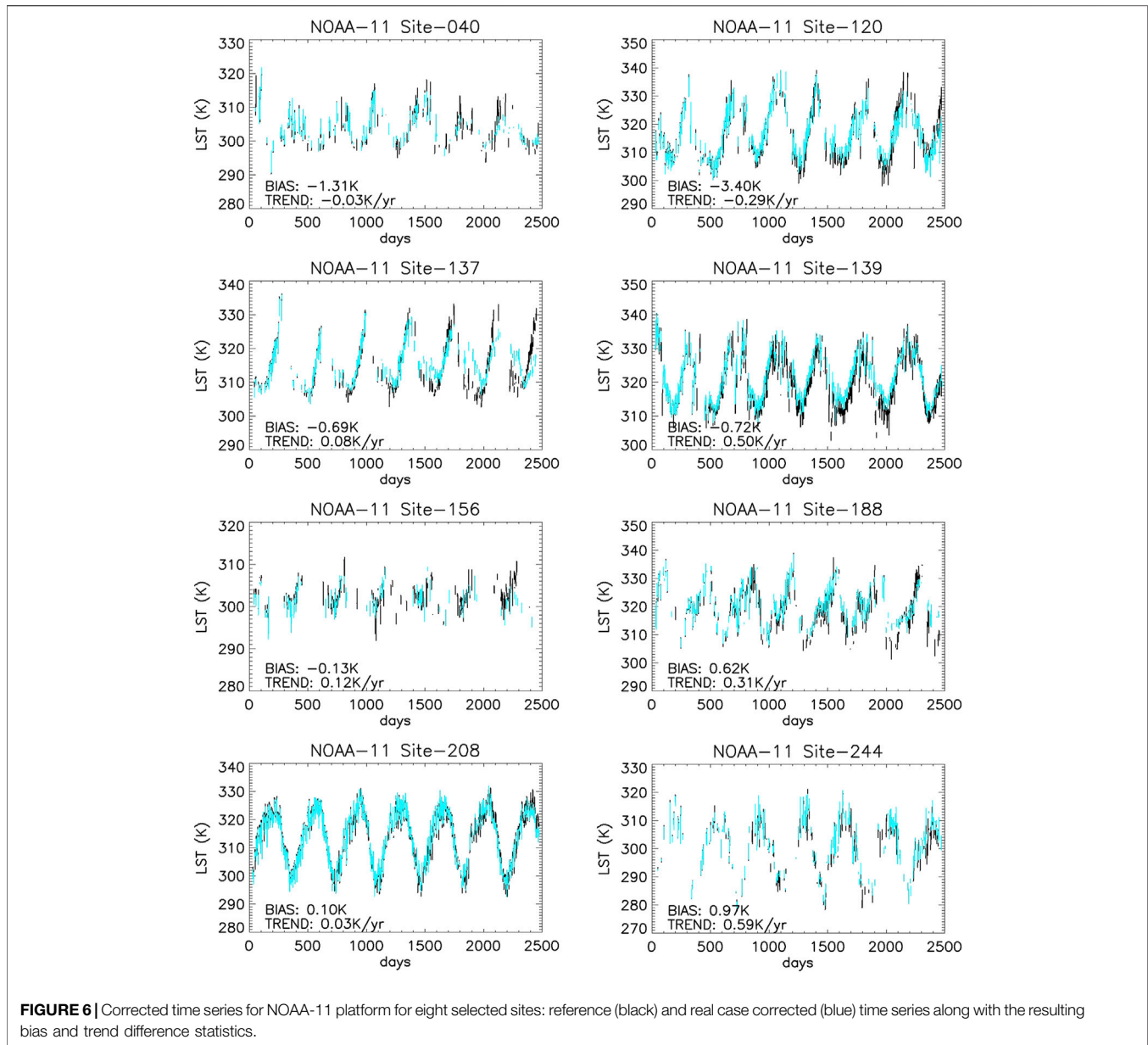
4.3 Statistics by Platform, Class, and Pixel

Figure 8 presents the histograms of bias and trend statistics for all sites and each satellite platform for raw data, as well as corrected time series in the ideal and real cases, and finally after Liu et al. (2019) correction. We see that bias and trend histograms are centered on 0 for NOAA-18 and 19 platforms in all cases, although bias values have a larger spread in the real case. For NOAA platforms 7 to 16, their bias and difference trend histograms present a strong deviation from zero before correction (smaller for NOAA-16), mostly removed after correction in both cases. We also observe that the spread of bias and trend statistics is stronger for NOAA-7 to 16. As for Liu et al. (2019) correction, both bias and difference trend histograms present a wide range of values (−5 to 10 K and −4 to 4 K/yr, respectively).

As for the histograms of bias and trend statistics by land cover (not shown), the small number of sites for most cases prevent from identifying clear behaviors for given classes. However, the desert land cover shows a coherent behavior for all corresponding sites, with bias values of −0.3 ± 0.1 K and difference trend values of −1.8 ± 0.5 K/yr before correction, of 0.0 ± 0.1 K and 0.0 ± 0.1 K/yr in the ideal case, and of 0.0 ± 1.0 K and 0.1 ± 0.3 K/yr in the real case, and −2 ± 2 K and −2 ± 2 K/yr for Liu et al. (2019) correction.

5 DISCUSSION

5.1 Insights

Our simulated time series provide new insights on orbital drift influence on LST time series. By subtracting the drifted from the

FIGURE 7 | Corrected time series for NOAA-11 platform for eight selected sites: reference (black) and Liu et al. (2019) corrected (red) time series along with the resulting bias and trend difference statistics.
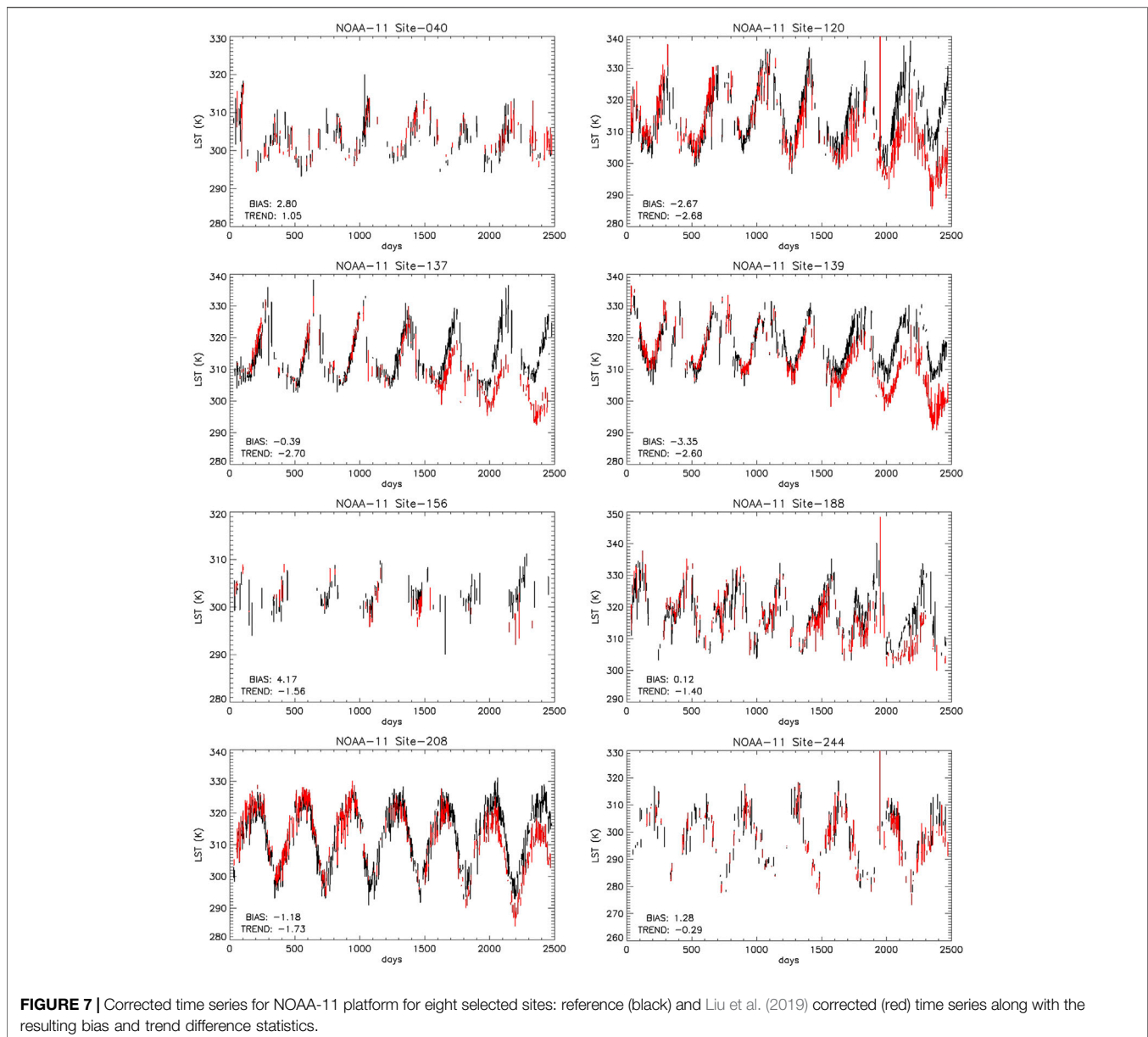
reference time series, we have evidenced a seasonal component of the orbital drift, ignored in previous statistical approaches. However, in real case applications, the noise in the drifted time series, due to changes in illumination and/or atmospheric conditions, prevented us from correcting this seasonal component.

This seasonal component results from a decrease in annual amplitude with time of the simulated drifted LST time series. This characteristic is logical, since the nominal orbit of NOAA platforms was chosen to coincide with daily maximum temperature. Therefore, a later overpass of the platform induces a decrease in retrieved LST (as evidenced by Price, 1990), although this decrease is not linear. Indeed, for a given pixel and similar delay, with a larger daily amplitude, summer LST estimates suffer from a major decrease than their winter counterparts, and therefore decrease the yearly amplitude of the drifted LST time series. This study is the first statistical approach to try and correct this effect, although some modeling and diurnal cycle approaches implicitly deal with it (Susskind et al., 1997; Jin and Treadon, 2003; Pinheiro et al., 2004; Liu et al., 2019).

On another hand, we have also shown that a key statistical parameter for orbital drift correction is the trend of the difference between reference and drifted time series. Alternative statistical parameters, such as standard deviation and RMSE, used in the literature, include both the influence of the orbital drift and inner characteristics of the time series. When comparing with *in situ* data, for coarse spatial resolutions such as NOAA AVHRR instruments, high standard deviation and RMSE values are common (see, for example, Liu et al., 2019), and can mask residual orbital drift effects.
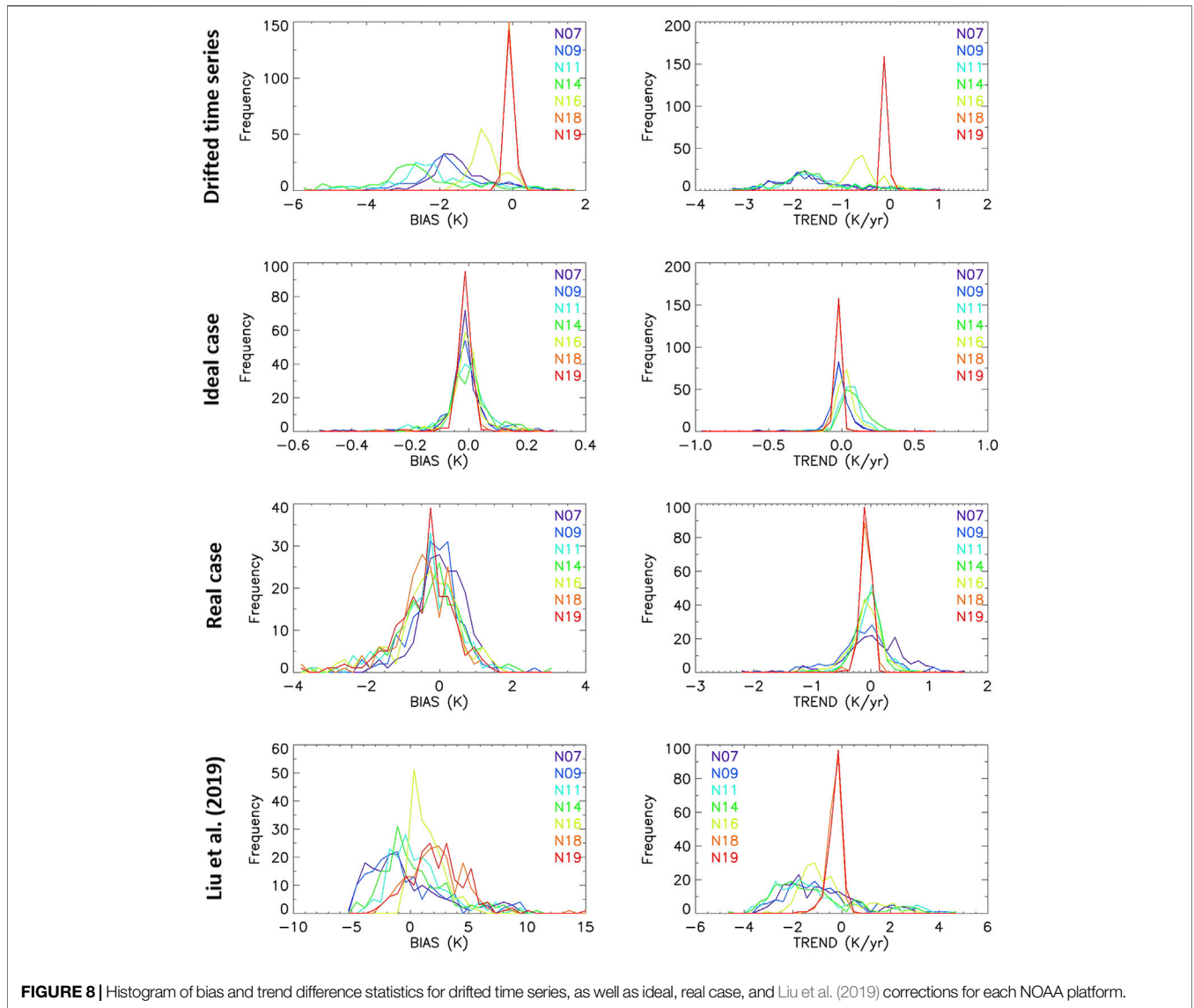
FIGURE 8 | Histogram of bias and trend difference statistics for drifted time series, as well as ideal, real case, and Liu et al. (2019) corrections for each NOAA platform.

Furthermore, **Figure 3** shows how the orbital drift effect can be evidenced for all pixels selected in **Table 7**, representative of most available land covers. In previous studies (Sobrino and Julien, 2016), the orbital drift effect has been said to have greater influence on given land covers (desert, semi-arid, croplands, etc). However, our results show that most sites suffer from this effect, with difference trend absolute values (up to 3 K/yr) largely above expected changes from global warming for example (maximum values of the order of 0.15 K/yr, see Sobrino et al., 2020a; Sobrino et al., 2020b).

5.2 Comparison of the Different Approaches

Among the three approaches studied here, the first approach, labeled ideal case, leads to the best results. The corresponding bias and difference trend values are close to zero, for most NOAA platforms, and thus hint toward a reliable correction of NOAA orbital drift effect. However, for real cases, the performance of the correction decreases slightly, although it remains higher than for the only other validated correction method (Liu et al., 2019).

We have seen that these results remain true for all NOAA platforms, although the remaining orbital drift effect varies with platform number. Since NOAA-16, platforms have been placed on an orbit that minimizes drift effect, at least for the first 3–4 years of operation. This leads to a lower need for orbital drift correction for these platforms, especially NOAA-18 and 19. However, in the recent LTDR-V5 dataset (Pedelty et al., 2007), NOAA-19 data span a period of more than 12 years. In that case, orbital drift correction will also be mandatory.

Liu et al. (2019) correction nevertheless improves on the drifted time series but falls short of removing it completely. This approach is based on the reconstruction of the LST diurnal cycle, by using the local heterogeneity of the fraction of vegetation cover. However, in most cases, at coarse spatial scale, the local heterogeneity of the fraction of vegetation cover is limited, and therefore the reconstruction of the LST diurnal cycle is hindered. The best example of this lies in desert areas, where this method cannot be carried out, due to a homogeneous null

fraction of vegetation cover. However, deserts are one of the land covers most influenced by the orbital drift effect.

5.3 Limits

Our approach is based on the LST data estimated at the Global Change Unit of the University of Valencia as described in Sobrino et al. (2020c). LST values for all 15-min acquisitions between 2013 and 2019 were retrieved for each pixel, from which both the reference and drifted time series were estimated. An objection to the correction we present here is that we use the same equation (d(t) equation in the Methods section) for both simulating the drifted time series and correcting them. We emphasize that this equation is used to select the LST values based on their acquisition times, and then as a baseline for drift fitting on temperature values. This could lead to an overestimation of the adequacy of the correction methods presented here. Straightforward application of our method to actual AVHRR data will provide more confidence in our results.

An alternative to this drawback could be to simulate data from the actual satellite equator crossing time, and not the approximation provided by Ignatov et al. (2004). Another alternative would be to compare the simulated time series with actual NOAA data. Finally, one could add noise to the simulated equator crossing times, thus considering the residuals of the fitting from which results Ignatov et al. (2004) equation. These are directions for future work.

On another hand, pixel spatial heterogeneity is not expected to have any influence on the correction, since its performance relies on the retrieval of fitting parameters, depending only on the pixel LST time series, and not its land cover class. However, pixel spatial heterogeneity may influence our analysis of the results by land cover. This can be addressed by selecting a higher number of pixels and checking method performance homogeneity within each IGBP class.

Additionally, the bias statistical parameter for our real case correction is suboptimal in most cases (up to 0.2 K in absolute value). However, classical intercalibration approaches between satellites can be carried out to remove this bias (Pedelty et al., 2007), by matching time series for overlapping periods for different NOAA platforms or by using alternative sensors (SPOT–Satellite Pour l'Observation de la Terre, MODIS–Moderate Resolution Imaging Spectroradiometer) when no overlapping periods are available.

Our results show that a complete correction of the orbital drift is feasible, provided a previous knowledge of the full influence of the drift on the LST time series. This knowledge can be approximated by using a geometrical model of the surface (Pinheiro et al., 2004) or by reconstructing the LST diurnal cycle (Susskind et al., 1997; Jin and Treadon, 2003; Liu et al., 2019). However, in the case of statistical approaches, such as our previous studies (Sobrino et al., 2008; Julien and Sobrino, 2012; Julien and Sobrino, 2021), this knowledge has to be approximated from an average year of data, or the first year of data as carried out here. Nonetheless, either an average or the first year of data still include some orbital drift effects, and therefore lead to a suboptimal correction of this orbital drift. There is therefore room for further improvements, where simulated data such as the ones used in this work are recommended.

6 CONCLUSION

In this study, we have simulated reference and drifted LST time series for 177 sites, representing various land covers, and seven NOAA afternoon platforms (7, 9, 11, 14, 16, 18, and 19). We have shown that the orbital drift effect is evidenced for most sites and not only specific land covers (desert, semi-arid areas, and croplands). We have selected the bias and trend of the difference between reference and drifted time series to assess the validity of an orbital drift correction, as better indicators than traditionally used standard deviation and RMSE.

We have analyzed the difference between reference and drifted time series and identified a seasonal component in the orbital drift, never identified in previous studies. We proposed an approach for orbital drift correction in an ideal case where the full orbital drift effect is known. In that case, overall bias is zero, with a standard deviation of 0.07 K, and overall difference trend value is 0.05 K/yr, with a standard deviation of 0.06 K/yr. These values are within reach of the stability specifications of LST as an ECV. However, in the actual panorama of validated orbital drift correction methods, our approach is definitively an improvement.

When actually correcting LST time series, the full orbital drift effect is unknown, and statistical corrections are based on the drifted time series alone. We proposed a simpler approach for that real case, where the seasonal component is omitted for the correction. This correction leads to a slight decrease of performance, with overall bias value of −0.13 K (standard deviation of 0.83 K), and a null overall difference trend (standard deviation of 0.33 K/yr).

These results were also analyzed for eight selected sites and compared with the only available correction method which had been validated against *in situ* data, with a performance clearly lower than both of our approaches. We explain this difference by methodological drawbacks in the case of coarse spatial resolution data. Finally, all results were also analyzed by satellite platforms, showing that the performance of the correction varied with the characteristics of the orbit the platforms were placed on.

Finally, we discussed how future orbital drift corrections could be improved, by considering its seasonal component, and by better identifying the full effect of the orbital drift on the drifted LST time series alone. These are the directions we plan to explore in future work.

DATA AVAILABILITY STATEMENT

The raw data supporting the conclusion of this article will be made available by the authors, without undue reservation.

AUTHOR CONTRIBUTIONS

Conceptualization: YJ; methodology: YJ; software: YJ; investigation: YJ; data curation: YJ; writing—original draft preparation: YJ; writing—review and editing: YJ and JS; visualization: YJ; supervision: JS; project administration: JS;

REFERENCES

Baret, F., Morissette, J. T., Fernandes, R. A., Champeaux, J. L., Myneni, R. B., Chen, J., et al. (2006). Evaluation of the Representativeness of Networks of Sites for the Global Validation and Intercomparison of Land Biophysical Products: Proposition of the CEOS-BELMANIP. *IEEE Trans. Geosci. Remote Sensing* 44, 1794–1803. doi:10.1109/tgrs.2006.876030

Derrien, M., and Le Gléau, H. (2005). MSG/SEVIRI Cloud Mask and Type from SAFNWC. *Int. J. Remote Sensing* 26, 4707–4732. doi:10.1080/01431160500166128

Gutman, G. G. (1999). On the Monitoring of Land Surface Temperatures with the NOAA/AVHRR: Removing the Effect of Satellite Orbit Drift. *Int. J. Remote Sensing* 20, 3407–3413. doi:10.1080/014311699211435

Hersbach, H., Bell, B., Berrisford, P., Hirahara, S., Horányi, A., Muñoz-Sabater, J., et al. (2020). The ERA5 Global Reanalysis. *Q.J.R. Meteorol. Soc.* 146, 1999–2049. doi:10.1002/qj.3803

Ignatov, A., Laszlo, I., Harrod, E. D., Kidwell, K. B., and Goodrum, G. P. (2004). Equator Crossing Times for NOAA, ERS and EOS Sun-Synchronous Satellites. *Int. J. Remote Sensing* 25, 5255–5266. doi:10.1080/01431160410001712981

Jin, M., and Treadon, R. E. (2003). Correcting the Orbit Drift Effect on AVHRR Land Surface Skin Temperature Measurements. *Int. J. Remote Sensing* 24, 4543–4558. doi:10.1080/0143116031000095943

Julien, Y., and Sobrino, J. A. (2012). Correcting AVHRR Long Term Data Record V3 Estimated LST from Orbital Drift Effects. *Remote Sensing Environ.* 123, 207–219. doi:10.1016/j.rse.2012.03.016

Julien, Y., and Sobrino, J. A. (2021). NOAA-AVHRR Orbital Drift Correction: Validating Methods Using MSG-SEVIRI Data as a Benchmark Dataset. *Remote Sensing* 13 (5), 925. doi:10.3390/rs13050925

Julien, Y., Sobrino, J. A., and Sòria, G. (2015). Retrieving and Broadcasting Near-Real-Time Biophysical Parameters from MODIS and SEVIRI Receiving Stations at the Global Change Unit of the University of Valencia. *Int. J. Remote Sensing* 36, 5273–5288. doi:10.1080/01431161.2015.1040134

Liu, X., Tang, B. H., Yan, G., Li, Z. L., and Liang, S. (2019). Retrieval of Global Orbit Drift Corrected Land Surface Temperature from Long-Term AVHRR Data. *Remote Sensing* 11, 2843. doi:10.3390/rs11232843

Pedelty, J., Devadiga, S., Masuoka, E., Brown, M., Pinzon, J., Tucker, C., et al. (2007). "Generating a Long-Term Land Data Record from the AVHRR and MODIS Instruments," in Proceedings of the 2007 IEEE Inter-national Geoscience and Remote Sensing Symposium, Barcelona, Spain, 23-28 July 2007, 1021–1025. doi:10.1109/igarss.2007.4422974

Pinheiro, A. C. T., Privette, J. L., Mahoney, R., and Tucker, C. J. (2004). Directional Effects in a Daily AVHRR Land Surface Temperature Dataset over Africa. *IEEE Trans. Geosci. Remote Sensing* 42, 1941–1954. doi:10.1109/tgrs.2004.831886

Pinheiro, A. C. T., Mahoney, R., Privette, J. L., and Tucker, C. J. (2006). Development of a Daily Long Term Record of NOAA-14 AVHRR Land Surface Temperature over Africa. *Remote Sensing Environ.* 103, 153–164. doi:10.1016/j.rse.2006.03.009

Pinzon, J., Brown, M. E., and Tucker, C. J. (2005). "Satellite Time Series Correction of Orbital Drift Artifacts Using Empirical Mode Decompo-Sition," in *EMD and its Applications.* Editors N. E. Huang and S. S. P. Shen (Toh Tuck, Singapore: World Scientific), 285–295.

Price, J. C. (1990). Using Spatial Context in Satellite Data to Infer Regional Scale Evapotranspiration. *IEEE Trans. Geosci. Remote Sensing* 28, 940–948. doi:10.1109/36.58983

Sobrino, J. A., and Julien, Y. (2016). Exploring the Validity of the Long-Term Data Record V4 Database for Land Surface Monitoring. *IEEE J. Sel. Top. Appl. Earth Obs. Remote Sensing* 9 (8), 3607–3614. doi:10.1109/JSTARS.2016.2567642

Sobrino, J. A., Julien, Y., Atitar, M., and Nerry, F. (2008). NOAA-AVHRR Orbital Drift Correction from Solar Zenithal Angle Data. *IEEE Trans. Geosci. Remote Sensing* 46, 4014–4019. doi:10.1109/tgrs.2008.2000798

Sobrino, J. A., Julien, Y., and García-Monteiro, S. (2020a). Surface Temperature of the Planet Earth from Satellite Data. *Remote Sensing* 12, 218. doi:10.3390/rs12020218

Sobrino, J. A., García-Monteiro, S., and Julien, Y. (2020b). Surface Temperature of the Planet Earth from Satellite Data over the Period 2003-2019. *Remote Sensing* 12, 2036. doi:10.3390/rs12122036

Sobrino, J. A., Julien, Y., Jiménez-Muñoz, J.-C., Skokovic, D., and Sòria, G. (2020c). Near Real-Time Estimation of Sea and Land Surface Temperature for MSG SEVIRI Sensors. *Int. J. Appl. Earth Obs. Geoinform.* 89, 102096. doi:10.1016/j.jag.2020.102096

Susskind, J., Piraino, P., Rokke, L., Iredell, L., and Mehta, A. (1997). Characteristics of the TOVS Pathfinder Path A Dataset. *Bull. Amer. Meteorol. Soc.* 78, 1449–1472. doi:10.1175/1520-0477(1997)078<1449:cottpp>2.0.co;2

Weedon, G. P., Gomes, S., Viterbo, P., Shuttleworth, W. J., Blyth, E., Österle, H., et al. (2011). Creation of the WATCH Forcing Data and its Use to Assess Global and Regional Reference Crop Evaporation over Land during the Twentieth century. *J. Hydrometeorol.* 12, 823–848. doi:10.1175/2011jhm1369.1